Printable Thermoelectric Device

Printable Thermoelectric Device

Printable Thermoelectric Device

K. Miyazaki[*], K. Kuriyama, and T. Yabuki

Department of Mechanical and Control Engineering, Kyushu Institute of Technology,
1-1 Sensui-cho, Tobata-ku, Kitakyushu, Fukuoka 804-8550, Japan.

[*]Email: miyazaki@mech.kyutech.ac.jp

Abstract. We have fabricated a printed flexible thermoelectric generator using composite of Bi_2Te_3 and PEDOT:PSS. The nano-structured thermoelectric thin film was made by printing method and the paste for printing was prepared by mixing nano-particles of Bi_2Te_3, PEDOT:PSS and polyamic acid as a additives. The non-dimensional figure of merit was 0.2 for p-type composite thin film at room temperature due to the low thermal conductivity. The interfacial thermal resistance between Bi_2Te_3 and PEDOT:PSS was measured to understand the low effective thermal conductivity of the printed thermoelectric composite. The measured organic-inorganic interfacial thermal resistance is in the order of 10^{-7} $(m^2 \cdot K)/W$ which is about 10 times higher than the inorganic-inorganic interfacial thermal resistance. The extremely low thermal conductivity of the printed thermoelectric materials can be explained by high interfacial resistance between inorganic-organic materials.

1. Introduction

The electricity can be directly generated from thermal energy by thermoelectric conversion even at room temperature. On the other hand, thermal energy can be transferred for cooling by applying the electricity to the thermoelectric material. The thermoelectric efficiency is the function of the non-dimensional figure of merit, ZT ($Z = \sigma S^2 / \lambda$, S: Seebeck coefficient (V/K), σ: Electrical conductivity (S/m), λ: Thermal conductivity (W/m·K), T: Temperature, (K)) [1]. Bismuth telluride (Bi_2Te_3) has shown one of the best performance for thermoelectric generator since its discovery [2]. However, transforming into flexible, printable and wearable electronics is challenging task while maintaining desired high ZT. To maintain a high ZT by lowering thermal conductivity, nano-structuring of a material has been reported from the view point of heat conduction [3]. The thermal energy is transported in solids by lattice vibration, and the mechanisms can be understood by phonon transport [4]. The heat conduction is diffusive when the characteristic size is much larger than mean free path of phonons. However, the ballistic phonons transport will occurs when the characteristic size is shorter than the mean free path of phonons. Thermal conductivity is no longer constant physical property under the ballistic phonon transport [5]. The figure of merit can be enhanced by using the difference between phonons and electrons mean free path [6]. The mean free path of electrons is mostly shorter than the mean free path of phonons. The phonon transport can be suppressed by nano-structures, such as nano-porous [7,8], nano-composite [9], nano-crystalline [10], nano-wire [6] etc. to enhance the value of ZT.

In this manuscript, we present the flexible thermoelectric electric module prepared by printing method and an understanding of thermal boundary resistance at the organic-inorganic interface which plays an important role in the reduction of effective thermal conductivity to enhance the figure of merit.

2. Interfacial Thermal Boundary Resistance Evaluation

Interfacial thermal resistance is determined using a differential 3ω method [11]. In this method, the value of thermal resistance can be obtained from the temperature rise (ΔT_{AC}) (Expressed by equation1) due to Joule heating, generated by applying an alternating current ($I=I_0\cos(\omega t)$) in a thin aluminum line wire on the sample. This aluminum line works as a heater and thermometer.

$$\Delta T_{AC} = \frac{P}{\pi\lambda_s}\left\{\frac{1}{2}ln\left(\frac{D_s}{b^2}\right) + 0.923 - \frac{1}{2}\ln(2\omega)\right\} + \frac{P}{2b}R_f \qquad (1)$$

where, λ_s is the thermal conductivity of the substrate, D_s is the thermal diffusivity of the substrate, R_f is the thermal resistance of the thin film sample, P is the power per unit length applied to the thin aluminum line wire, and 2b is the width of the aluminum wire. The first term of the equation (1) reflects the thermal physical property of the substrate while the second term is the contribution from thin film. In our analysis, sample is linear connections of resistance in the series where we can simple subtract the resistance equation to get the value of interfacial resistance. Applying the same analysis, the thermal resistance of the thin film can be written as equation (2) by subtracting the temperature change (equation (1)) for the substrate and the thin film on the same substrate (substrate + thin film).

$$R_f = \frac{\Delta T_f - \Delta T_s}{I_0^2 R_0} A \qquad (2)$$

where, ΔT_f is the temperature rise of the sample (substrate + thin film), ΔT_s is the temperature rise of the substrate, A is the surface area of the aluminum thin wire, and R_0 is the resistance of this aluminum wire. The solution of equations (1) and (2) can be written as equation (3) where δ is the thickness of the thin film and λ is the thermal conductivity of the thin film. We can estimate the value of interfacial thermal resistance (R_i) from the y-intercept of the plot of film thickness and thermal resistance [12].

$$R_f = \frac{\delta}{\lambda} + R_i \qquad (3)$$
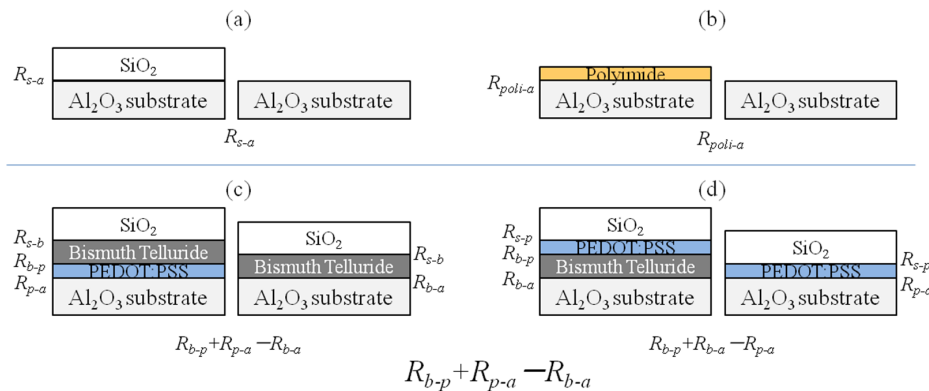

Fig.1: Schematic for thermal boundary resistance (a) for SiO$_2$-Al$_2$O$_3$ boundary resistance, (b) for Polyimide-Al$_2$O$_3$ boundary resistance, (c) and (d) for Bi$_2$Te$_3$-PEDOT:PSS boundary resistance.

Figure 1 shows a schematic diagram of the series of samples. We subtract the resistance connected in series to get the organic-inorganic interfacial boundary resistance. Alumina was used as a substrate due to its relatively high thermal conductivity. We calculated thermal boundary resistance at the

interface of SiO_2 and alumina substrate (R_{s-a}) by subtracting measured thermal resistance of SiO_2 thin film (R_s) and alumina substrate (R_a). Similarly, we calculated thermal boundary resistance at the interface of polyimide and alumina substrate (R_{poli-a}) (Fig.1 (a) and (b)). In a simple notation, we used suffix *poli* for polyimide, *a* for an alumina substrate, and *s* is SiO_2 thin film. Further, the interfacial thermal boundary resistance of Bi_2Te_3-PEDOT:PSS was calculated by two cases. In the first case, the thickness of PEDOT: PSS was varied while the thickness of SiO_2 and Bi_2Te_3 were kept constant (Fig 1 (c)). Thermal boundary resistance at the interface of Bi_2Te_3 and PEDOT:PSS ($R_{b-p}+R_{p-a}-R_{b-a}$) was obtained in Fig. 1 (c). The suffix *p* indicates PEDOT:PSS, and *b* indicates Bi_2Te_3. In case two, the thickness of Bi_2Te_3 was varied while keeping the thickness of PEDOT:PSS and SiO_2 constant (Fig 1 (d)). The interfacial thermal resistance $R_{b-p}+R_{b-a}-R_{p-a}$ was obtained (Fig 1 (d)). Interfacial thermal resistance R_{b-p} of Bi_2Te_3 and PEDOT: PSS was obtained by adding interface thermal resistance $R_{b-p}+R_{p-a}-R_{b-a}$ and $R_{b-p}+R_{b-a}-R_{p-a}$.

3. Experimental Detail

We fabricated organic-inorganic interface of PEDOT:PSS-Bi_2Te_3, the organic-inorganic interface of the polyimide-alumina substrate and the inorganic-inorganic interface of the SiO_2-alumina substrate. PEDOT: PSS, Bi_2Te_3, polyimide, and SiO_2 thin films were prepared on alumina substrate for respective interface thermal resistance measurement. A polyimide film was prepared by spin coating. Thick polyamic acid solution (16 wt %) (Sigma Aldrich) was diluted in N-methyl-2-pyrrolidone. It was stirred for 10 mins to achieve a homogeneous solution to be used in spin coating. The thickness of polyimide film is about 500, 700, 1,000 and 1,800 nm. PEDOT:PSS thin films are also spin coated on plasma treated alumina substrate. The rotation speed was changed to produce 60 and 105 nm thin films. Bi_2Te_3 is used as an inorganic thermoelectric material for organic-inorganic interface. The thin film of Bi_2Te_3 of thickness 100, 330, and 560 nm was deposited by arc plasma technique in a vacuum chamber at the base pressure of 5.0×10^{-3} Pa on alumina substrate [13]. The deposition was carried out by performing a predetermined number of discharges at a discharge voltage of 80 V and a discharge interval of 1 second. The growth rate is about 0.8 nm per discharge. Thermal conductivity of the thin films is measured by 3ω technique. We deposited thin aluminum metal line wire by thermal deposition technique using a shadow mask in a vacuum chamber (5.0×10^{-3} Pa) to serve as a heater and temperature sensor. SiO_2 was deposited as an insulator in between sample and aluminum wire by e-beam evaporation technique.

4. Results and Discussion

Figure 2 shows thin film of composite of Bi_2Te_3 and PEDOT:PSS on a flexible substrate. There are many interfaces between organic and inorganic materials. The measured thermal conductivity was 0.2-0.3 W/(m·K)[14]. It was much lower than the evaluated value by using conventional thermal conductivity model for composite. We summarize the result of thermoelectric organic-inorganic interface in figure 3. The temperature rise of PEDOT:PSS on alumina substrate is shown in Fig 3 (a) while thickness of Bi_2Te_3 and SiO_2 films are kept constant about 400 and 800 nm respectively. The temperature rises with increase in thickness. The thermal resistance variation depending on the thin film thickness of PEDOT: PSS are shown in Fig 3 (b). The thickness of PEDOT: PSS thin film was varied from 50 nm to 100 nm while thickness of Bi_2Te_3 and SiO_2 films is kept constant about 400 and 800nm respectively. The thermal conductivity of PEDOT: PSS was 0.34±0.13 W/(m·K) (literature value 0.3 W/(m·K) [15]).
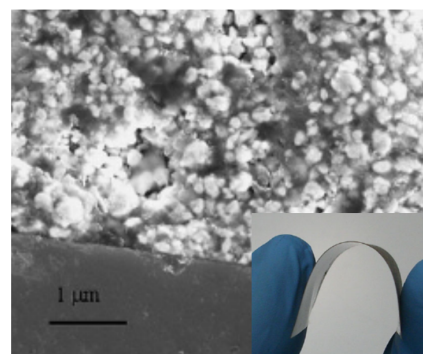

Fig.2: SEM cross-sectional image of a printed Thin film of composite of Bi_2Te_3 and PEDOT:PSS. Inset: Thin film of composite of Bi_2Te_3 and PEDOT:PSS on a flexible substrate.

The interfacial thermal resistance $R_{b-p}+R_{p-a}-R_{b-a}$ obtained from the y-intercept of Fig. 3 (b) was $1.9 \pm 0.4 \times 10^{-7}$ (m$^2 \cdot$K)/W. The temperature rise of Bi$_2$Te$_3$ on the alumina substrate of Fig.3 (c), while PEDOT: PSS (100 nm) and SiO$_2$ (2000 nm) are kept constant. The obtained thermal resistance and the film thickness of Bi$_2$Te$_3$ are shown in Fig 3 (d). The thermal conductivity of Bi$_2$Te$_3$ was 1.3 ± 0.13 W/(m·K) (literature value 1.5 W/(m·K) [1]). The interfacial thermal resistance $R_{b-p}+R_{b-a}-R_{p-a}$ obtained from the y-intercept of Fig. 3 (d) was $2.6 \pm 2.0 \times 10^{-8}$ (m$^2 \cdot$K)/W. The Bi$_2$Te$_3$-PEDOT: PSS interface thermal resistance R_{b-p} was about $1.1 \pm 1.2 \times 10^{-7}$ (m$^2 \cdot$K)/W.

The thermal conductivity of polyimide thin films is about 0.6 ± 0.2 W/(m·K) (literature value 0.2 W/(m·K) [16]). The thermal conductivity of polyimide is closely related to the microstructure, and further discussion on the difference between the literature value and the experimental value is under investigation. The interfacial thermal resistance R_{poli-a} of the polyimide- alumina substrate interface is about $4.3 \pm 3.4 \times 10^{-7}$ (m$^2 \cdot$K)/W. The measured thermal conductivity of SiO$_2$ is about 1.02 ± 0.4 W/(m·K) (literature value 0.7 W/(m·K) [17]). The interfacial thermal resistance R_{s-a} of the SiO$_2$-alumina substrate interface is about $4.1 \pm 4.0 \times 10^{-8}$ (m$^2 \cdot$K)/W. Our result shows that the organic-inorganic interfacial thermal resistance is 10 times higher than the inorganic-inorganic interfacial thermal resistance.
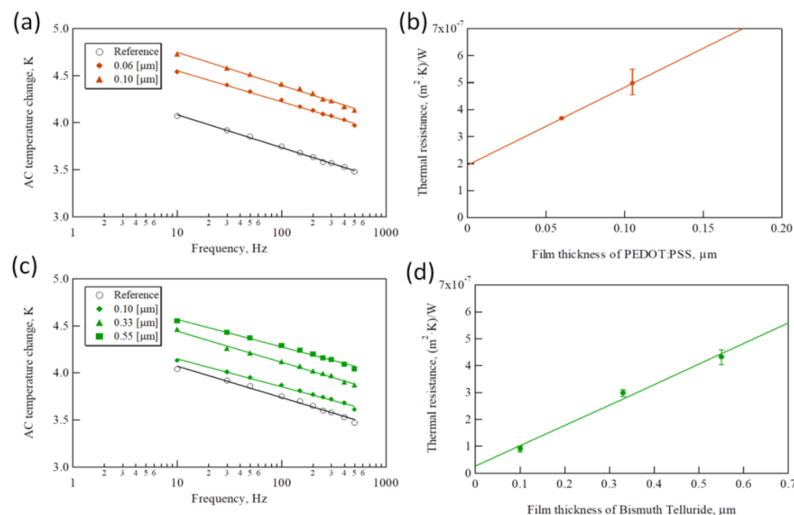

Fig.3: (a) AC temperature change and (b) thermal resistance of multilayered thin films with different thickness of PEDOT:PSS while thickness of Bi$_2$Te$_3$ and SiO$_2$ films are kept constant about 400 and 800 nm respectively, (c) AC temperature change and (d) thermal resistance of multilayered thin films with different thickness of Bi$_2$Te$_3$ while the thickness of PEDOT:PSS and SiO$_2$ films are kept constant about 100 and 2000 nm respectively.

5. Summary

We have successfully fabricated a printed flexible thermoelectric thin film using a composite of an organic and inorganic hybrid (Bi$_2$Te$_3$, PEDOT:PSS). Our result shows the value of ZT for the composite of Bi$_2$Te$_3$, PEDOT:PSS was 0.2 for p-type at room temperature. Further, the interfacial thermal resistance was determined in the series of samples such as alumina substrate-polyimide thin film, alumina substrate-SiO$_2$ thin film, alumina substrate-PEDOT: PSS-Bi$_2$Te$_3$-SiO$_2$ thin film, alumina substrate-Bi$_2$Te$_3$-PEDOT: PSS-SiO$_2$ thin films. We found that the thermal resistance of the alumina substrate-polyimide interface was $4.3 \pm 3.4 \times 10^{-7}$ (m$^2 \cdot$K)/W, the interface thermal resistance of the alumina substrate-SiO$_2$ interface was $4.1 \pm 4.0 \times 10^{-8}$ (m$^2 \cdot$K)/W. The thermal resistance of the organic-inorganic interface is 10 times larger than the thermal resistance of the inorganic-inorganic interface,

and it is found that the thermal resistance is great among materials having completely different properties. The thermal resistance of the Bi_2Te_3-PEDOT: PSS interface was $1.1\pm0.3\times10^{-7}$ (m^2·K)/W. We believe it will serve as a new path for establishing a method to predict heat conduction in organic-inorganic hybrid system.

References
1. Rowe D M 1995 CRC Handbook of Thermoelectrics, CRC press.
2. Chung D Y, Hogan T, Schindler J, Iordarridis L, Brazis P, Kannewurf C R, ... & Kanatzidis M G 1997 Proceedings ICT'97. XVI International Conference on (pp. 459-462). IEEE.)
3. Snyder G J, Toberer E S 2008 Nature materials **7** 105-114.
4. Majumdar A 1993 Journal of heat transfer **115** 7-16.
5. Cahill D G, Wayne K F, Mahan G D, Majumdar A, Maris H J, Merlin R, Phillpot S R 2003 Journal of applied physics **93** 793-818.
6. Hochbaum A I, Chen R, Delgado R D, Liang W, Garnett E C, Najarian M, Majumdar A, Yang P 2008 Nature **451** 163-167.
7. Kashiwagi M, Hirata S, Harada K, Zheng Y, Miyazaki K, Yahiro M, Adachi C 2011 Applied physics letters **98** 023114.
8. Kato K, Hatasako Y, Uchino M, Nakata Y, Suzuki Y, Hayakawa T, Adachi C, Miyazaki K 2014 Advanced materials interfaces 1300015.
9. Heremans J P, Jovovic V, Toberer E S, Saramat A, Kurosaki K, Charoenphakdee A, Yamanaka S, Snyder G J 2008 Science **321** 554-557.
10. Poudel B, Hao Q, Ma Y, Lan Y, Minnich A, Yu B, Yan X, Wang D, Muto A, Vashaee D, Chen X, Liu J, Dresselhaus MS, Chen G, Ren Z 2008 Science **320** 634-638.
11. Cahill D G 1990 Rev. Sci. Instrum., **61** 802 .
12. Kim j H, Feldman A, Novotny D 1999 J. Appl. Phys., **86** 3959.
13. Uchino M, Kato K, Hagino H, Miyazaki K 2013 J. Electron. Mater. **42** 1814-1819.
14. Kato K, Hagino H, Miyazaki K 2013 Journal of electronic materials**. 42(7):**1313-1318.
15. Liu J, Wang X, Li D, Coates N E, Segalman R A, Cahill D G 2015 Macromolecules **48(3)** 585-591.
16. Li TL, Hsu SL.2010 the Journal of Physical Chemistry B. **114(20):**6825-9.
17. Yamane T, Nagai N, Katayama SI, Todoki M. 2002 Journal of applied physics. **91(12):**9772-6.